Research Square

Preprints are preliminary reports that have not undergone peer review.
They should not be considered conclusive, used to inform clinical practice,
or referenced by the media as validated information.

Experimental Thermal-Hydraulic Analysis of Double-Pipe Exchanger with Helical Fins and Al_2O_3/Water Nanofluid

Firas Aziz Ali
Technical Engineering Collage of Mosul, Northern Technical University
Ahmed Hani Ghanim
ahmed.hanigh@ntu.edu.iq
Technical Engineering Collage of Mosul, Northern Technical University
Asmaa Taha Ahmed
College of Engineering, University of Mosul,
Mohammed Taha Luhaibi
Technical Engineering Collage of Mosul, Northern Technical University

Research Article

Keywords: Double-pipe heat exchanger, Helical fins, Al_2O_3 nanofluid, Nusselt number, Pressure drop, Performance Evaluation Criterion, Thermal-hydraulic performance

Posted Date: June 29th, 2026

DOI: https://doi.org/10.21203/rs.3.rs-9868693/v1

License: This work is licensed under a Creative Commons Attribution 4.0 International License.
Read Full License

Additional Declarations: No competing interests reported.

Experimental Thermal-Hydraulic Analysis of Double-Pipe Exchanger with Helical Fins and Al_2O_3/Water Nanofluid

Firas Aziz Ali[1] Ahmed Hani ghanim[1] Asmaa Taha Ahmed[2] Mohammed Taha Luhaibi[1]

[1]Department of Power Techniques Engineering, Technical Engineering Collage of Mosul, Northern Technical University, Mosul 41001, Iraq
[2]Department of Mechanical Engineering, College of Engineering, University of Mosul, Mosul 41001, Iraq

Corresponding author email:ahmed.hanigh@ntu.edu.iq

Abstract

The heat transfer and flow characteristics of a counter-flow double-pipe heat exchanger with internal helical fin-tubes using Al_2O_3/water nanofluids in turbulent flow conditions at nanoparticle concentrations of 0.25-1.25% volumetric fraction were examined experimentally. The Nusselt number (Nu), overall heat transfer coefficient (U) and pressure drop (ΔP) were calculated, and the Performance Evaluation Criterion (PEC) was used to evaluate the system's performance.

It was found that the finned-tube design led to a significant enhancement in heat transfer. The highest Nu value (32.5) and U (1078.9 $W/m^2 \cdot K$) were obtained at 0.25% and 1.25% concentrations, respectively. While the pressure drop increased gradually with higher nanoparticle concentrations (up to 3.44 kPa), the PEC values for all test conditions were greater than 1.0, with a maximum value of 1.33, demonstrating the overall thermodynamic improvement in all cases.

Overall, the integration of internal helical fins with Al_2O_3 nanofluids provides an effective approach for enhancing compact heat exchanger performance. Experimental results agreed with established correlations, confirming consistent thermal-hydraulic behavior. The combined effects of fin-induced secondary flow and nanoparticle micro-convection produced greater enhancement than either technique alone. Thus, the proposed hybrid configuration offers a practical solution for improving heat recovery and thermal management

Keywords: Double-pipe heat exchanger; Helical fins; Al_2O_3 nanofluid; Nusselt number; Pressure drop; Performance Evaluation Criterion; Thermal-hydraulic performance

1. Introduction

Rising energy demand, driven by industrialization and population growth, places mounting pressure on thermal engineering. The finite nature of fossil fuel reserves and tightening emission targets [1],[2]. Necessitate improved performance from heat exchangers. The primary limitation often lies with the working fluid (e.g., water, ethylene glycol, oils), as these are poor thermal conductors compared to modern materials and the requirements of compact systems [3] [4]. As such, researchers are searching for new improvement strategies to guarantee optimum energy recovery and apparatus size reduction [5], [6].

The double pipe heat exchanger (DPHE) serves as the ideal test platform for these concepts, owing to its simple geometry, ease of instrumentation, and ability to withstand high operating pressures. This combination of accessibility and structural robustness makes it a logical starting point before scaling passive enhancement strategies to more complex configurations.[7], [8]. Smooth-tube DPHEs with pure fluids can no longer meet growing heat demands. The challenge is to strike a balance where convective heat transfer improvements greatly exceed hydraulic losses due to flow resistance[9], [10].

An easy and passive method to increase heat transfer in double-pipe exchangers is to add helical fins to the inner pipe to increase surface area, promote more fluid mixing, and no moving parts. [11], [12] ,[13], [14] ,[16], [17].

The literature on process intensification has recently analyzed the advantages of using helical and spiral forms of curved design. Recent research on twin-coil heat exchangers has shown that spiral arrangements maximize fluid turbulence helping to design extended tube lengths within confined spaces. In spiral designs, the changing radius of curvature has a direct bearing on the secondary flow behavior and the overall thermal-hydraulic efficiency. Also, the addition of radial or annular fins on the outside of these coils can increase the heat transfer coefficient by 69% over unfinned systems. This improvement occurs due to the intermittent disruption of the boundary layer, along with the generation of secondary vortices in the shell-side fluid. While these design changes increase the convective rates, they also increase the pressure drop due to the increase in surface friction and flow path extension [6], [15], [17].

Geometry is among the more sure levers towards breaking the thermal boundary layer. Rinik et al. (2025). **Rinik et al. (2025)** [18] numerically tested a DPHE with a fully twisted inner pipe and conical ring tabulators at Re = 5,000-26,000. The swirl drove fluid toward the heated wall in a consistent manner and the results show it: Nu peaked at 445 with a counter-flow condition, and the maximum PEC was 2.3. The twisting of pipes together with secondary tabulators obviously works well at high velocities. The same story can be told by surface depressions. **Cao et al. (2021)**[19] introduced circular depressions to both tubes of a double helical exchanger and measured the entropy generation and exergy performance. There was a notable enhancement of thermal transport across smooth helical baselines, which would be expected, as curved flow channels already introduce an effective load in the boundary layer, and surface interactions would be expected to strengthen that effect, in contrast to fighting it.

Nakhchi et al. (2021) [20] went experimental and fitted DPHEs with double-perforated inclined elliptical tabulators through Re = 5,000-18,000. The holes formed recirculation areas and forced fluid between the core and the wall where thermal resistance

is concentrated. The increase in Nu (217.4 percent) compared with the plain-tube base, the increase in friction factor (143.1 percent), and the highest efficiency parameter (1.849) were recorded. Within the conditions of the test, the thermal gain was reasonably strong in comparison to the hydraulic penalty. Fin morphology is crucial; it is not solely the presence of fins[21] , but also the fin shape itself. **Piran et al. (2024)** [21] demonstrated this with spiral V-shaped axial fins.

Zonouzi (2026)[22] used an alternate geometry, helical dual-pass coaxial systems with axial fins, and reported that fin-assisted conduction reduced phase change time by up to 15.7%. Both findings both indicate the same result that the shape of the fin varies the result, not its contribution to the total surface area.

The literature on process intensification has recently analyzed the advantages of using helical and spiral forms of curved design. Recent research on twin-coil heat exchangers has shown that spiral arrangements maximize fluid turbulence helping to design extended tube lengths within confined spaces. In spiral designs, the changing radius of curvature has a direct bearing on the secondary flow behavior and the overall thermal-hydraulic efficiency. Also, the addition of radial or annular fins on the outside of these coils can increase the heat transfer coefficient by 69% over unfinned systems. This improvement occurs due to the intermittent disruption of the boundary layer, along with the generation of secondary vortices in the shell-side fluid. While these design changes increase the convective rates, they also increase the pressure drop due to the increase in surface friction and flow path extension [23]. Parallel to the fin geometry work, nanofluids emerged to overcome the thermal conductivity ceiling of conventional fluids. Al_2O_3 dominates the literature due to its thermal, chemical, and economic advantages.[11], [14], [24], [25].

Hussien et al. (2021)[26] conducted experiments on a DPHE with Al2O3 and CuO nanoparticles in engine oil. Both types of particles at 0.05% and 0.1% increased the heat transfer coefficient proportionally to loading. On the conductive side the alumina stood up well. This was further pushed by **Ahirwar and Kumar (2026)**[15] to (CuO + ZnO)-water hybrid nanofluids at 0.1%-1.0%. Enhanced stability compared to single-component fluids, and with optimized geometry, Nu increased by 281.87% at peak conditions. Combining two types of particles, in the investigated range, always performed better than either of the materials. The validations of Al2O3/water in double-pipe types across 0.1%-0.4% volume ratio were done by **Naseema et al. (2018)**[3]**.** The overall ratio of the heat transfer coefficient improvement was 1.305, a reasonable value given the loading level. The ceiling is equally important as the floor, however.

However, the upper limit of concentration is equally important **Peng et al.** (2025) [24]] found that when concentration was increased to 5.90% in helical structures, viscosity rose sufficiently to completely negate the thermal benefit, reducing the heat transfer rate by 12.6%. This highlights that an inadequate nanoparticle concentration yields an insignificant impact, while an excessive concentration can cause the fluid to act against itself by increasing viscosity. The experimental optimum lies somewhere between these two failure modes, and finding that experimentally (not by conjecture) provides precisely the kind of useful data for scholarly research.

In a shell-and-two-coil exchanger, **Alizadeh et al. (2026)** [6] combined annular fins with SiC-CNT hybrid nanofluid. Average Nu was 69 percent above baseline, PEC was at the peak at 2.28. The fins increase the surface area; the nanofluid promotes micro-

convection and most importantly, in the conditions of the experiments under consideration, neither effect suppressed the other.

Assaf et al. (2025)[27] loaded a heat exchanger tube with ring inserts and twisted tape, and introduced Al_2O_3 -CuO/water hybrid nanofluid at 0.9% volume fraction. The convective heat transfer coefficient was further increased by the nanofluid alone by 18.2 percent over the increase that the inserts accomplished. The thermal performance factor increased by 1.38 to 3.29. Neither the geometry nor the fluid gets there by itself that gap is the entire case to unite them. The same story is told with spiral geometries, **Al-Asadi et al. (2026)**[11] simulated double helical coils with the help of Al_2O_3 -TiO_2 hybrid nanofluid and reported Nu increases of up to 136 percent over standard coils, with PEC holding around 2.2 at lower Reynolds numbers. **Hameed et al. (2026)**[13] took a completely different approach by employing Archimedean spiral piped heat exchangers with ZnO/water nanofluid, achieving a PEC of approximately 3.95. This value is notably high and approaches the upper range reported for passive hybrid enhancement techniques in recent studies. While the result is impressive, its true validity depends on experimental verification under real operating conditions rather than relying solely on numerical predictions. Finally, **Nam et al. (2023)**[14] put this out numerically and studied Al_2O_3 nanofluids in a double-pipe helical coil at 1.0% volume fraction. The coefficient of heat transfer was 1.43 times better than water, the factor of performance was 1.4. Pressure drop was raised, but not sufficiently to counteract the thermal gain

There are very few experimental data on the interaction of fin-induced swirl with nanoparticle micro-convection in a finned DPHE; most of the existing data is numerical [6], [14], [27]. Whether or not helical fins can change the distribution of nanoparticles and their stability in suspension under turbulent flow, and whether the thermal gain is worth the hydraulic resistance, is truly open to debate. And there is a second gap to be named. Most experiments operate at small volume fractions in laminar flow, which leaves behavior at higher volume fractions up to 1.25% in turbulent regimes that have not been extensively studied[8], [24]. It is not yet agreed upon which concentration of Al_2O_3 actually optimizes PEC in finned geometries. Physical datasets of Al_2O_3 with helical fins in a real dual-pipe rig are sparse; the major part of similar work is done with SiC-CNT or a hybrid form of metal oxide in various configurations[6],[9],[17]. The only way to bridge that gap is to run experiments with a wide variety of Reynolds numbers and concentrations, not simulations. This study aims to experimentally address these gaps.

We directly compared the thermal and hydraulic performance of finned and plain-tube configurations, measured over a range of operating conditions, recording the overall heat transfer coefficient, Nusselt number, pressure drop, and PEC, and compared these performance parameters directly to isolate the contribution of each of the enhancement mechanisms. The dataset measures how the secondary flow caused by the fin and nanoparticle micro convection interact and whether the increase in the heat transfer gains due to the interaction of the two types of micro convection. We also discussed the transitional regime, $1000 < Re < 4000$, that receives less experimental interest than fully turbulent flow despite being directly relevant to low velocity industrial systems. The flow in this regime is sensitive to perturbations, and we found it to be accelerated by helical fins in transitioning to turbulence compared to smooth-tube baselines, which is what we validated against the existing empirical correlations and against the previous work of Aghayari et al.[28]

Table 1 : Overview of the recent studies on heat transfer enhancement by nanofluids, and passive methods.

Author & Year	Enhancement Type	Nanofluid Used	Key Improvement (%)
Al-Asadi (2026)[11]	Double Helical Coil	Al_2O_3-TiO_2/Water	Nu up 136%
Assaf (2025)[27]	Rings + Twisted Tape	Al_2O_3-CuO/Water	TPF up to 3.29
Nam (2023)[14]	Helical Coil DPHE	Al_2O_3/Water	Nu ↑ 43% (1.43× water)
Karouei (2024)[8]	Shell/Double Coil	MgO-TiO_2/Water	η up 51.7%
Piran (2024)[21]	Spiral V-shaped Fins	PCM/NEPCM	Charging up 186%
Ahirwar (2026)[15]	Wire Coil Inserts	CuO+ZnO/Water	Nu up 281.87%
Alizadeh (2026)[6]	100 Annular Fins	SiC-CNT/Water	PEC = 2.28
Rinik (2025)[18]	Elliptical Twisted Pipe	Pure Water	PEC = 2.3
Ben Said (2025)[16]	Perforated Turbulator	Al_2O_3-TiO_2/Water	h up 42%
Hameed (2026)[13]	Archimedean Spiral	ZnO/Water	PEC = 3.95
Naseema (2018)[3]	Smooth DPHE	Al_2O_3/Water	Uo up 30.5%
Nakhchi (2021)[20]	Perforated Elliptic	Pure Water	Nu up 217.4%
Chaurasiya (2024)[29]	V-cut Twisted Tape	SiO_2/Water	Nu up 87.73%
Hussien (2021)[26]	Smooth DPHE	Al_2O_3/CuO in Oil	Nu up 15-17%
Zonouzi (2026)[22]	Helical dual-pass	Axial Fins	Time reduction 15.7%

The trend as observed in Table 1 is difficult to overlook. Geometric alterations with nanofluids. Consistently have higher performance than either method individually Nu improvements of up to 281% and PEC. More than 3.9 under perfect conditions are not outliers; they appear frequently throughout. Independent studies. The trend applies irrespective of whether the geometry is helical, spiral, or finned: passive methods. Do not work as well out of groups as they work in groups. Al_2O_3 nanofluids in combination with helical or spiral fins, in the range of the studied, seem to be a very efficient combination to compact Exchanger design. The literature has not tackled with caution fixed internal fins most published work. It is based on removable inserts or twisted tapes, which add contact resistance and fouling. Fears that permanently incorporated fins evade altogether. It is that gap that we aim at here. The PEC value is constantly greater than unity in the previous research, which provides decent confidence that the approach is something that one should experiment with, not merely calculate.

2. Methodology

2.1. Heat Exchanger Description and Geometry

The section of the test was a horizontal counter-flow double-pipe heat exchanger, particularly to maximize the logarithmic mean temperature difference between the working lengths. The inner tube is made of copper, which is selected to ensure the minimum conductive thermal resistance. The outer shell is CPVC, which has thermal insulation to contain heat exchange between the two working.

Liquids instead of seeping into the environment. As shown in Figure 1, the inner copper tube features permanently fixed helical fins that extend radially into the annular space. Here, permanent integration is important. Resistance to contact, no movement in the presence of flow, and no fouling gaps that can be removed by inserts.

The fins perturb the thermal boundary layer and create the second swirling flows. That enhances convective heat transfer. The fabricated assembly is shown in Figure 2. CPVC shell, instrumentation, and finned inner tube. Precise positioning was achieved with custom spacers. Any eccentricity shifts the local flow pattern and spoils the heat transfer coefficients; this step was not optional. The inlet and outlet calming zones ensured hydrodynamically full development. Conditions in front of the fluid entering the part of the test. We conducted experiments in $1000 < Re < 4000$, most of which were in the transitional regime, which is more chaotic and random than completely turbulent flow. The tested conditions under which the value of the element was tested are as follows: helical fins always hastened the process of transition to turbulence relative to a smooth tube. Baseline, which is a part of what makes this geometry interesting at lower flow velocities. As shown in Table 2, the test section was configured as a horizontal counter-flow double-pipe heat exchanger.

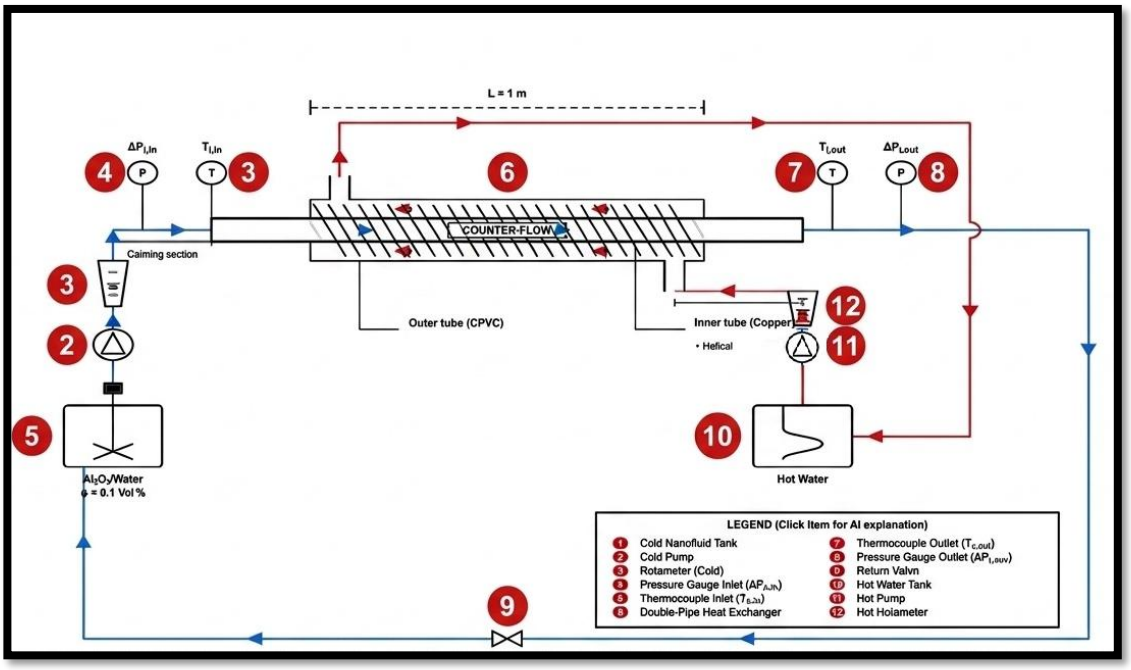


Figure 1 : Schematic diagram of the experimental counter-flow double-pipe heat exchanger test rig.

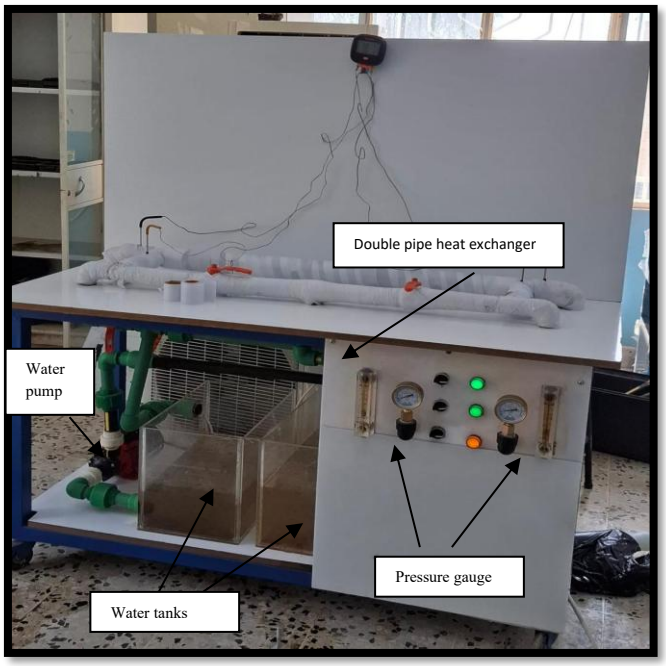


Figure 1 :Photograph of the actual experimental test rig showing the double-pipe heat exchanger, helical finned inner tube (inset), pumps, and instrumentation.

Table 2: Geometric specifications of the double-pipe heat exchanger

Parameter	Value	Unit
Outer tube internal diameter (ID)	22.3	mm
Outer tube external diameter (OD)	54	mm
Annular gap	13.85	mm
Effective heat transfer length	1000	mm
Inner tube wall thickness	2.0	mm
Inner tube wall thickness	2.0	mm
Outer tube material	CPVC (thermally insulated)	-
Inner tube material	Copper	-
Flow arrangement	Counter-flow	-
Test rig frame length	1.5	m
Test rig frame width	1.0	m
Test rig frame height	1.5	m

2.2. Helical Finned Tube Specifications

To intensify convective heat transfer, the finned tubes are made of copper, with a base tube diameter of 22.3 mm and a wall thickness of 2 mm. These tubes are further modified with external helical fins having a pitch of 20 mm and an overall outer diameter (over the fins) of 22 mm, as illustrated in Table 3. The helical-fin geometry promotes boundary-layer disruption and induces Dean-vortex-driven secondary flow, which increases fluid mixing near the wall and intensifies heat transfer[30], [31], [32], [34], effectively transporting core fluid toward the heated wall while promoting radial mixing through centrifugal forces[16]. Unlike longitudinal fins, the helical orientation increases fluid residence time and enhances cross-sectional temperature uniformity[11]. The fins were permanently integrated into the tube's internal surface to eliminate contact resistance associated with removable inserts. This configuration specifically evaluates the synergistic interaction between geometry-induced macro-turbulence and nanoparticle-induced micro-convection in Al_2O_3/water nanofluid. Figure 3 shows the schematic illustration of the helical fin geometry, while Figure 4 presents the actual fabricated heat exchanger used in the experimental work.

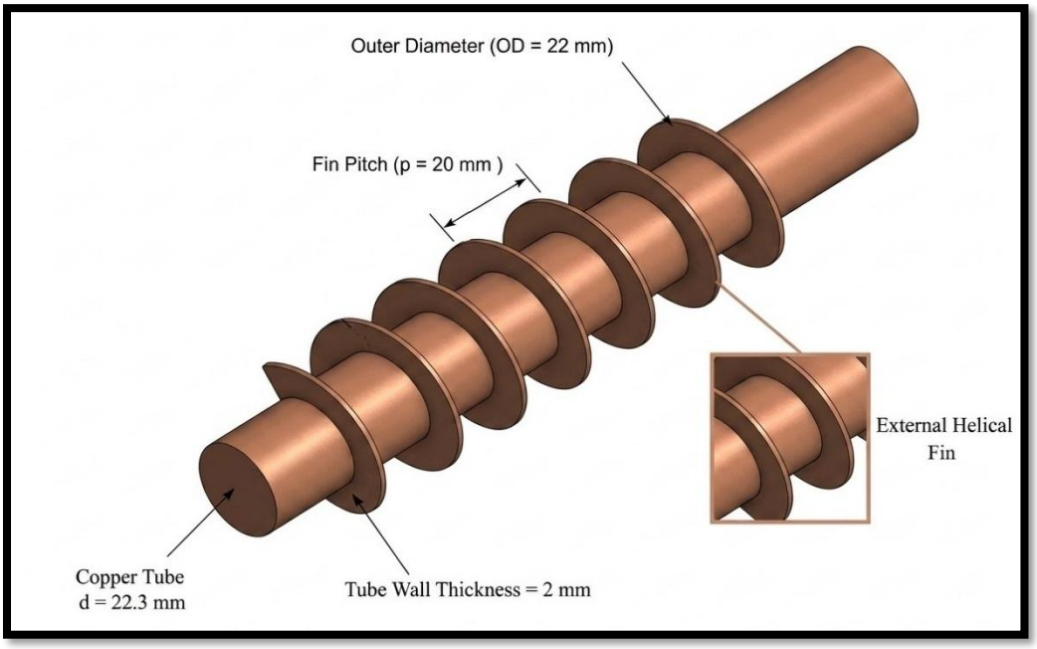


Figure 3 : Schematic diagram of the helical finned tube heat exchanger.

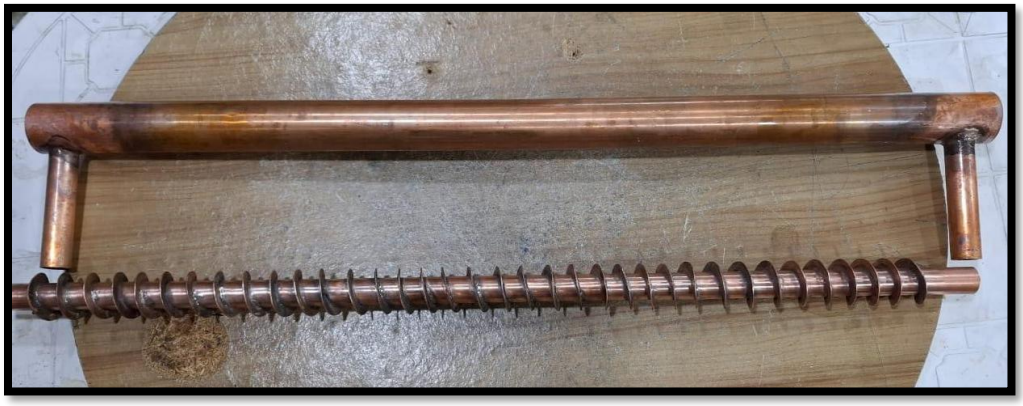


Figure 4: Experimental of the fabricated heat exchanger.

Table 3 : Annular Helical Fin Specifications

Parameter	Symbol	Value
Tube Length	L	1000 mm
Number of Fins	N	37
Fin Thickness	t	2 mm
Fin Height	h	11 mm
Fin Spacing	p	20 mm
Location	—	Annulus (between tubes)

2.3. Nanofluid Preparation and Characterization

The Al_2O_3-water nanofluid was prepared by the two-step method, in which pre-synthesized aluminum oxide nanoparticles were dispersed directly into distilled water to obtain the required volume concentration. Based on surfactant screening reported in the literature for Al_2O_3 nanofluids, sodium dodecyl sulfate (SDS) was selected as the surfactant due to its performance in previous comparative studies [34], [35]. The properties of SDS, detailed in Table 5, were accounted for during data reduction. In the present work, Al_2O_3 nanoparticles with the properties listed in Table 4 were used, namely a density of 3.89 g/mL, a particle size of 13 nm, a purity of 99.5%, a nearly spherical shape, and a white color. To calculate the required nanoparticle mass for volume concentrations ø = 0.25%, 0.5%, 0.75%, 1.0% and 1.25%, the law of mixtures was applied[15], [24]:

$$ø = \frac{Vnp}{Vnp + Vbf} \quad (1)[34]$$

The experiments in this study were conducted in the laboratories of Northern Technical University (NTU) using five samples as shown in Figures 5 and 6. Before preparation, the required mass of nanoparticles was calculated to achieve the desired nanofluid concentration, and the surfactant was added at a small dosage relative to the nanoparticle concentration to improve wettability and reduce the tendency of particle clustering. The mixture was first pre-dispersed using a magnetic stirrer for 15 min, following the procedure commonly used in the literature for surfactant-assisted nanofluid preparation. The suspension was then subjected to ultrasonic treatment using a CODYSON CD-4820 digital ultrasonic cleaner to break down any remaining agglomerates and produce a more uniform dispersion. The CD-4820 unit used in this study is a 2.5 L digital ultrasonic cleaner with a SUS304 stainless-steel tank, 5 timer settings, 38 kHz frequency, and a heating function up to 65°C, which makes it suitable for laboratory cleaning and dispersion applications.

After sonication, every batch was visually inspected for sedimentation or phase separation before it went near the test rig. This is not merely a formality; nanofluid stability directly affects measured thermal conductivity and viscosity, as an unstable suspension yields irreproducible data. We also prepared a surfactant-free reference sample alongside each SDS-assisted batch to directly assess the stability difference, following the approach recommended in previous nanofluid studies. The Al_2O_3/water suspension was sonicated for 2 hours before each experimental run. No visible sedimentation was observed during the testing period. The stability of the suspension was investigated by recording and maintaining pH within an acceptable range. This strategy yielded better results compared to a single reading, particularly over extended periods. The critical concentrations for the onset of visible settling were also determined. The thermophysical properties were considered, and normal values of these properties were chosen for a reference base fluid. Literature references demonstrate that the thermal conductivity and viscosity of water-based suspensions are desirable. For the simulation of the Al_2O_3/water suspensions, the Maxwell-Garnett and Brinkman models were used [40]. These models can be applied to low-concentration nanofluids where $\varphi \leq 1.25\%$. All reported thermal-hydraulic performance parameters (Nusselt number, overall heat transfer coefficient, pressure drop, PEC) were determined directly from the experimentally recorded temperatures, flow rates, and pressure drops.

Table 4: Properties of the nanoparticles.

Item	Specification
Nanoparticle	Al_2O_3
Particle size	13 nm
Density	3.89 g/mL
Purity	99.5%

Item	Specification
Shape	Nearly spherical
Surfactant	SDS
Reason for surfactant	Improve stability and reduce agglomeration
Stirring time	15 min
Sonication time	30 min
Ultrasonic cleaner	CODYSON CD-4820
Frequency	38 kHz
Tank capacity	2.5 L
Heating function	65°C max

Table 5: Properties of the surfactants.

Surfactant	Chemical Name	Type	Purity (%)	Density (g/mL)	Charge	Solubility in Water
Triton X-100	octylphenol ethoxylate	nonionic	≥99	1.07	neutral	high
PVA	polyvinyl alcohol	nonionic	≥98	1.25	neutral	high
Tween 80	polyethylene glycol sorbitan monooleate	nonionic	≥95	1.06	neutral	high
CTAC	Cetyltrimethylammonium chloride	cationic	≥98	0.90	+	medium
PVP	polyvinylpyrrolidone	nonionic	≥99	1.22	neutral	high
SDS	sodium dodecyl sulfate	anionic	≥99	1.01	-	high

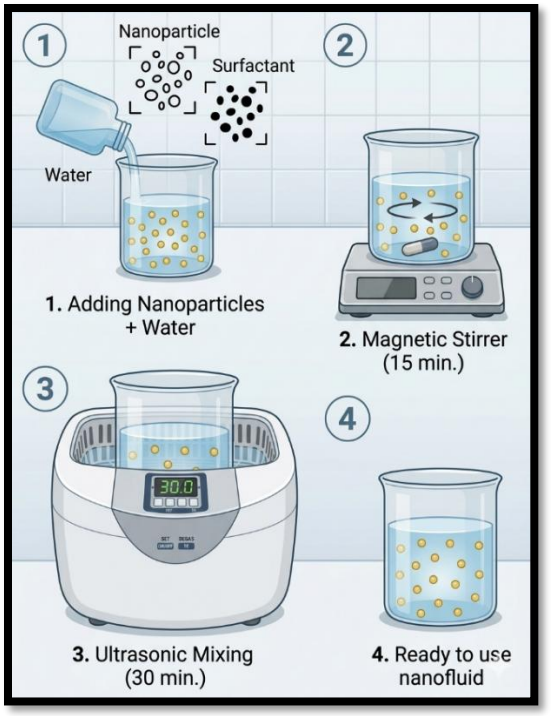


Figure 5: Nanofluid preparation

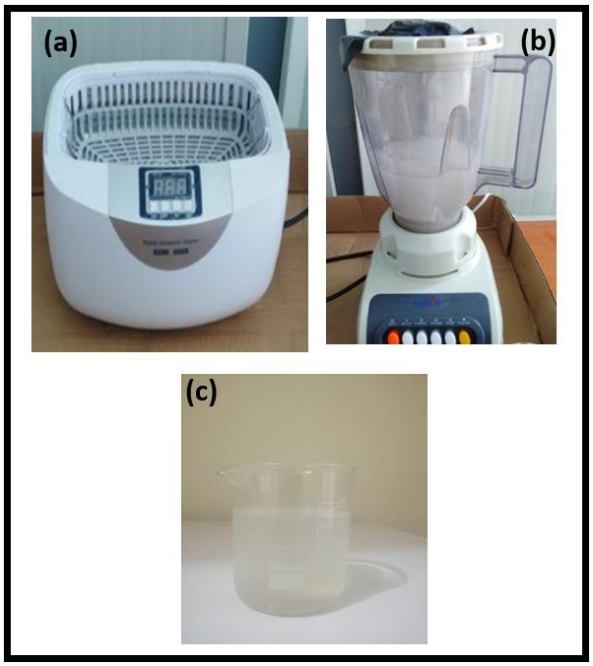


Figure 6: Prepared nanofluids using an ultrasonic homogenizer. (a) Ultrasonic cleaner (b) Magnetic stirrer(c) Prepared Al2O3/water nanofluid

2.4. Experimental Procedure

The experimental protocol began by filling the storage tanks with the working liquids and activating the heating mechanisms to achieve the desired inlet temperature of 50-60°C.[15]. Once the hot nanofluid and cooling water reached their set points, centrifugal

pumps were activated to circulate the fluids in a counter-flow configuration. The nanofluid flow rate was adjusted between 3 and 10 LPM to cover a range of Reynolds numbers. Steady-state conditions were confirmed when inlet and outlet temperature fluctuations did not exceed ±0.1°C over 15 minutes [36], [37]. Flow rates, temperatures, and pressure drops across the test section were recorded for each combination of volume concentration and flow rate. To ensure data reliability and reproducibility, each experimental point was repeated three times, and mean values were used for further calculations. Between runs involving nanofluids, the system was extensively flushed with deionized water to prevent any nanoparticle deposition on the tube walls.

2.5 Validation of Experimental Rig

Before running any nanofluid tests, we validated the rig using pure water in the smooth-tube configuration, the only honest way to know whether the setup is measuring what you think it is. Nusselt number data were compared against the Gnielinski correlation, and friction factor data against Blasius[38]. Maximum deviation across all tested conditions came in under ±5%. However, there was enough correlation with existing data to be able to formulate an acceptable base, although the validation data were kept handy during the entire process in case the values seemed too high or low.

2.6. Data Reduction

The thermal performance parameters were determined from the measured flow rates, inlet and outlet temperatures, and pressure drop using standard energy balance and heat transfer relations. The heat transfer rate for each fluid stream was calculated as. [20], [39]

"In the finned configuration, the hydraulic diameter (D_h) was calculated based on the annular flow area and wetted perimeter, and utilized in all dimensionless numbers (Re, f) to account for the geometric modifications introduced by the helical fins.

$$Q = \dot{m} Cp \Delta T \tag{2}$$

Where m is the mass flow rate, Cp is the specific heat capacity, and ΔT is the temperature difference between the inlet and outlet of the corresponding stream. The average heat transfer rate was obtained by taking the average of the hot-side and cold -side heat transfer rates. [20], [29], [39]

$$Qavg = \frac{(Qh + Qc)}{2} \tag{3}$$

The overall heat transfer coefficient (U) was determined using the Logarithmic Mean Temperature Difference (LMTD) method. [24], [26], [39], [40]

$$U = \frac{Qave}{(A \times LMTD)} \tag{4}$$

$$\text{LMTD} = \frac{(T_{h,\text{in}} - T_{c,\text{out}}) - (T_{h,\text{out}} - T_{c,\text{in}})}{\ln\left(\frac{T_{h,\text{in}} - T_{c,\text{out}}}{T_{h,\text{out}} - T_{c,\text{in}}}\right)} \quad (5)$$

Where A is the surface area (m^2), and the subscripts represent the hot and cold fluid inlet/outlet states. The overall heat transfer coefficient, U, was first determined from the measured heat duty using the LMTD method. To isolate the hot-side coefficient, hi*hi*, the thermal resistance network was then applied by considering the tube wall resistance and the annular-side resistance in series. In the present study, the outer-side heat transfer coefficient, h_o, was not assumed; instead, it was evaluated independently from the measured annular-flow conditions using a suitable empirical correlation for the external water flow. The resulting h_o value was then substituted into Eq. (6) to calculate h_i for each experimental run. The thermal performance parameters were obtained based on the flow rate, inlet and outlet temperature, and pressure drop values using energy balance and heat transfer equations. [15], [20]

$$h_i = \frac{1}{\frac{1}{U} - \frac{d_i \ln\left(\frac{d_o}{d_i}\right)}{2k_w} - \frac{d_i}{d_o} h_o} \quad (6)$$

The dimensionless Nusselt number (Nu) was calculated to characterize the convective transport efficiency. [39], [40]

$$\text{Nu} = \frac{h \cdot d_i}{k} \quad (7)$$

Where di is the inner diameter and k is the thermal conductivity of the fluid. The flow regime was identified using the Reynolds number (Re). [20], [27]

$$\text{Re} = \frac{\rho \cdot V \cdot d_i}{\mu} \quad (8)$$

Where ρ is the density, V is the mean velocity, and μ is the dynamic viscosity. The friction factor (f) was derived from the measured pressure drop (ΔP). [15], [29]

$$f = \frac{2\, d_i\, \Delta P}{\rho\, L\, V^2} \quad (9)$$

Where L is the length of the test section. The net energy benefit was evaluated using the Performance Evaluation Criterion (PEC), also known as the thermal performance factor. [8]

$$\text{PEC} = \frac{\text{Nu}/\text{Nu}_0}{(f/f_0)^{1/3}} \quad (10)$$

Where the subscript 0 refers to the baseline smooth tube results. Additionally, the Effectiveness-NTU method was used to assess the heat exchanger's thermal capability[20], [39], [22], [40]

$$\varepsilon = \frac{Q_{\text{act}}}{Q_{\text{max}}} \tag{11}$$

Where Q_{act} is the actual heat transfer and Q_{max} is the maximum possible heat transfer for the given flow conditions.

2.7. Uncertainty Analysis

To ensure the statistical validity of the findings, we performed a propagated uncertainty analysis based on the method proposed by Kline and McClintock. The individual errors for the independent variables were determined from the manufacturer's specifications and calibration data. Specifically, temperature measurements had an uncertainty of ±0.1 °C, while the flow rate and pressure drop recorded errors of ±1.0% and ±4.0%, respectively. The total uncertainty for the derived dimensionless parameters was calculated using the square root of the sum of the squares of the partial derivatives[15], [39].

$$w_R = \left[\left(\frac{\partial R}{\partial X_1}\cdot w_1\right)^2 + \left(\frac{\partial R}{\partial X_2}\cdot w_2\right)^2 + \cdots + \left(\frac{\partial R}{\partial X_n}\cdot w_n\right)^2\right]^{1/2} \tag{12}$$

Where w_R is the total uncertainty and w_n is the uncertainty of each independent variable. The maximum uncertainties for the Reynolds number are indicated by the analysis of the experimental data. This process was performed for all smooth and finned geometries, as well as all nanofluids, in order to clearly divide the thermal resistance and accurately evaluate the convective performance on the inner side.

3. Results and Discussion

The data set reflects the entire thermal-hydraulic performance of the DPHE with Al2O3 nanoparticles at a Reynolds number of 1000-4000, mostly in the transitional state. In this range, the fluid flow is highly sensitive, making its prediction difficult compared to the turbulent flow condition, hence the importance of the current results. The trends of the Nusselt number indicate that helical fins consistently induce turbulence at a lower Reynolds number compared to the smooth tube baseline.

The observed enhancements arise from two coupled mechanisms. First, the swirl generated by the helical geometry disrupts the thermal boundary layer and intensifies radial mixing, effectively driving the core fluid toward the heated wall. Second, nanoparticle motion (particularly Brownian diffusion and micro-convection) contributes to additional energy transport at the microscale, beyond what can be captured by bulk thermophysical properties alone. Under the investigated conditions, these effects appear to act

concurrently, with no evident suppression of either contribution. A quantitative separation of these mechanisms is presented in the following section.

3.1. Analysis of Nusselt Number and Reynolds Number

The relationship between Nu and Re allows for a conclusion concerning convection heat transfer properties, as shown in Figure 7. It is evident that for the smooth tube, the Nu grows with the rise in Re value, which is explained by a slow development of turbulence. To prove the validity of the measurements performed during experiments, the values of Nu were compared to the known correlation, the so-called Gnielinski correlation[38], It should be noted that in the range $1000 < Re < 4000$, which is examined in the experiment, the Dittus-Boelter correlation becomes unsuitable for calculations due to transitional flow effects. The agreement is sufficiently good, which allows stating the reliability of experimental data. In addition, based on the results obtained, it is possible to conclude that the flow regime examined here is transitional, not fully turbulent.

In a transitional flow regime, fins of the double coil design have been proven to increase turbulence onset Reynolds numbers compared to a smooth tube. This phenomenon has been demonstrated even in the graphs showing the dependence of Nu on Re. According to calculations, a 25-30% enhancement was revealed. This is caused by strong centrifugal forces created by the helical fin shape. As a result, secondary swirl flow develops, which contributes to radial mixing and thus makes cooling more efficient by moving cool fluid towards the surface being heated. At the same time, the thermal boundary layer formation is slowed down. It is possible to see from Figure 8 that this result coincides with the findings of N. Sreenivasalu Reddy et al.[41] .

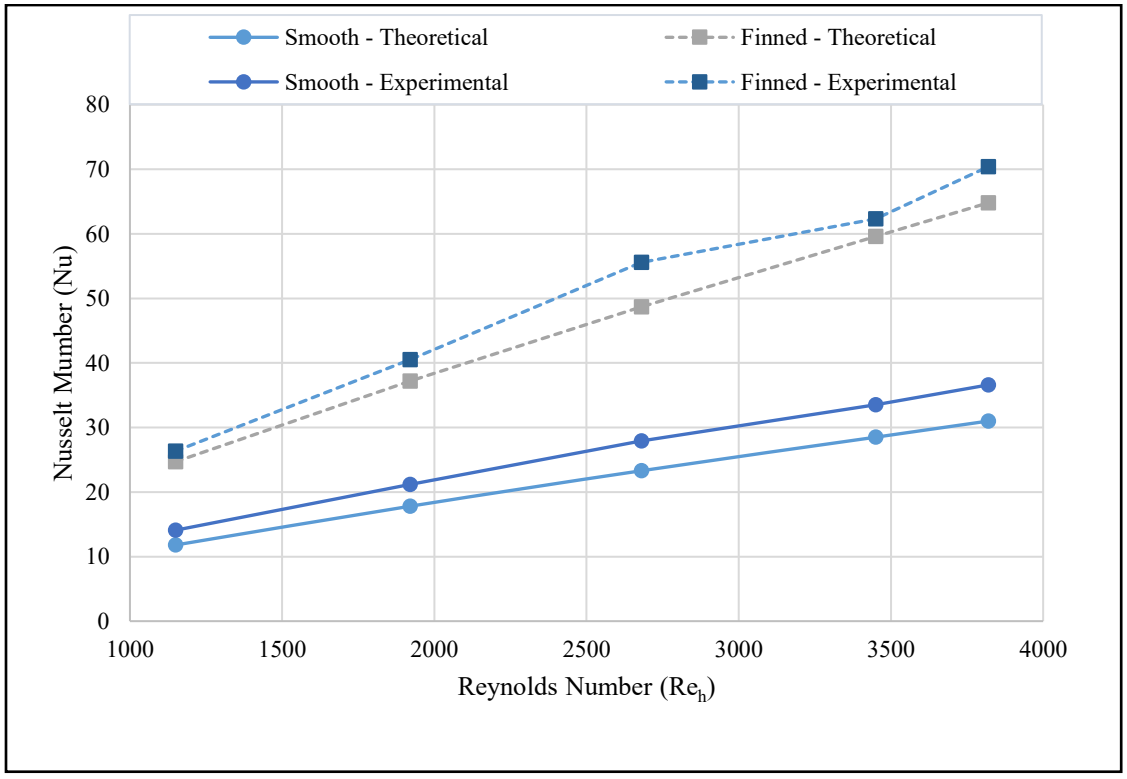


Figure 7: Experimental and theoretical Nusselt number (Nu_h) versus Reynolds number (Re_h) for the smooth and finned annulus (hot water side). Gnielinski correlation shown for smooth baseline validation.

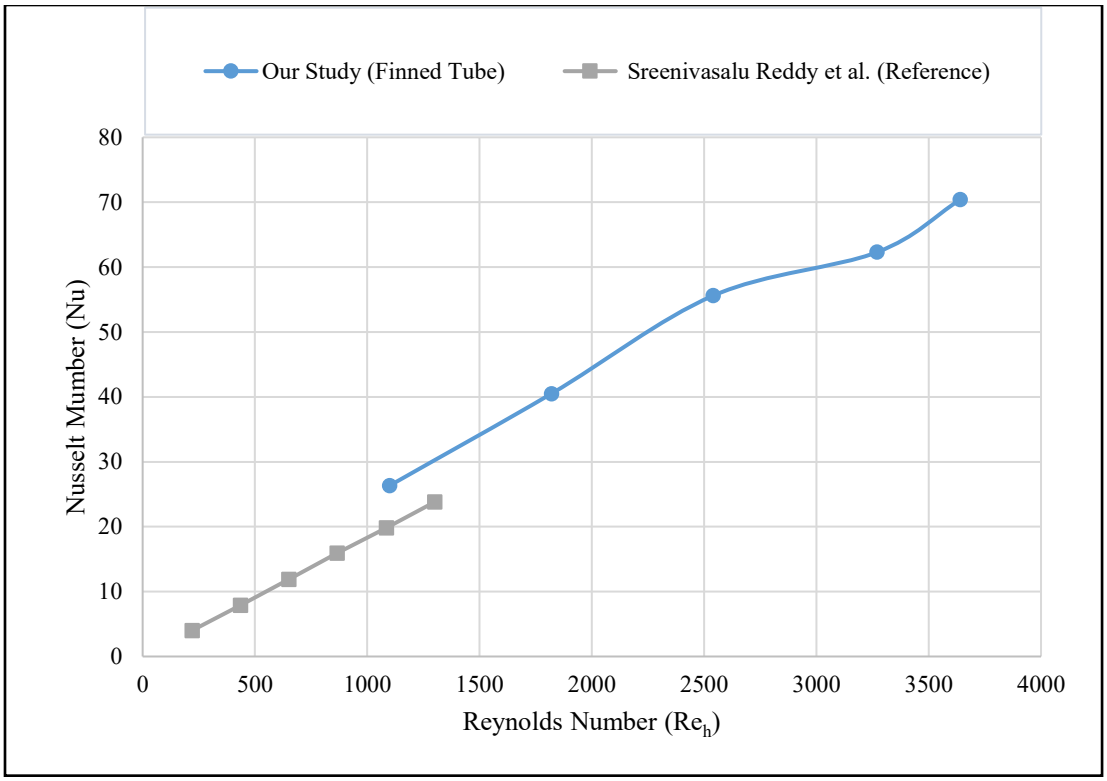


Figure 8: Validation of experimental Nu_h results against N. Sreenivasalu Reddy et al.[41] reference study for helical coil configurations. Peak reported in double coil geometry.

3.2. Influence of Al_2O_3 Volume Concentration

Figures 9 and 10, the use of Al_2O_3-water nanofluids results in a noticeable increase in hot-side Nusselt number (Nu_h), with the enhancement depending on the nanoparticle volume fraction (φ=0.25-1.25 vol.%) and Reynolds number (Re_h=1000-4000).

In the smooth tube (Figure 9), the Nusselt number increases from ~10–26 at φ=0.25% to 10.6–26.7 at φ=1.25%. This corresponds to an average increase of ~48%. The increase is primarily due to the higher thermal conductivity of the nanofluid and micro-mixing induced by Brownian motion, which weakens the viscous sublayer.

In contrast, the response of the helically finned tube is stronger. As shown in Figure 10, the Nusselt number increases from 12.4 to 32.5 at φ=0.25% to even higher values at φ=1.25%. In this case, the enhancement is attributed to swirl flows generated by the fins, which increase nanoparticle transport in regions of strong temperature gradient near the tube wall through the thermophoretic effect, resulting in enhanced heat transfer

In comparison with the work of Aghayari et al.,[28] which reported smooth-tube Al_2O_3-water measurements (particle size of 20 nm, φ=0.1-0.3 vol.%) resulting in Nusselt numbers of 19-25 at Re_h ≈13,000-27,000, the present work reaches similar maximum Nusselt numbers ($Nu_{h,max}$≈27) at approximately one-tenth of those Reynolds numbers. The data of Aghayari et al. show that the Nusselt number reaches a plateau after Re_h > 20,000, since, at those Re numbers, inertia plays a dominating role, while nanoparticles have almost no influence on heat transfer anymore. Contrary to their results, current experimental data diverge in the transitional Reynolds number range, where the Nusselt

number continues increasing instead of reaching a plateau, which implies effective interaction between the particles and the fluid at low Reynolds numbers where inertial effects do not dominate yet.

This difference might be caused by dispersion quality. For φ=1.25%, it is vital to achieve good dispersion of the suspension. Each batch underwent sonication of 2 hours. Also, pH of the fluid was controlled with great accuracy, since it was shown before [24] that agglomeration under high shear rate could lead to failure. Proper dispersal helps bring about Brownian motion and micro mixing, while aggregation works mainly to increase drag. The difference between these two conditions is very great indeed. For the current system, the pumping efficiency rises seven and a half times for an equivalent increase in heat transfer.

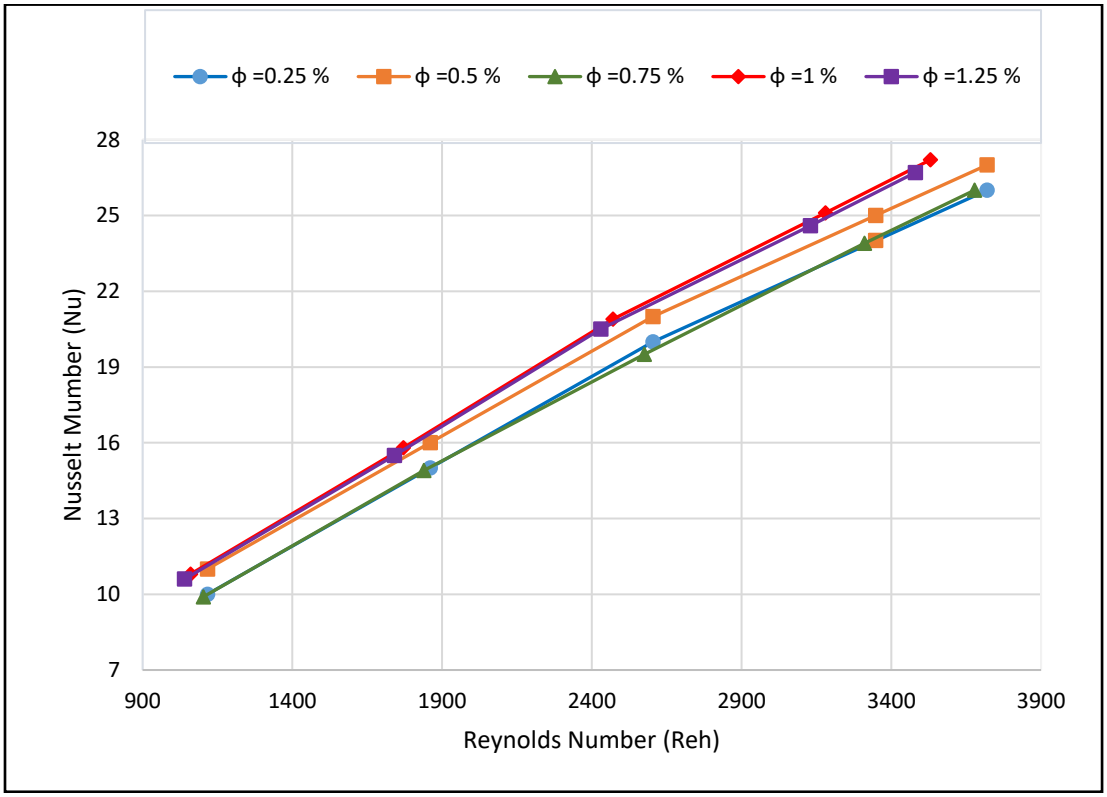


Figure 9: Nusselt Number (Nu) vs. Reynolds Number (Re) for different nanofluid concentrations in a smooth tube

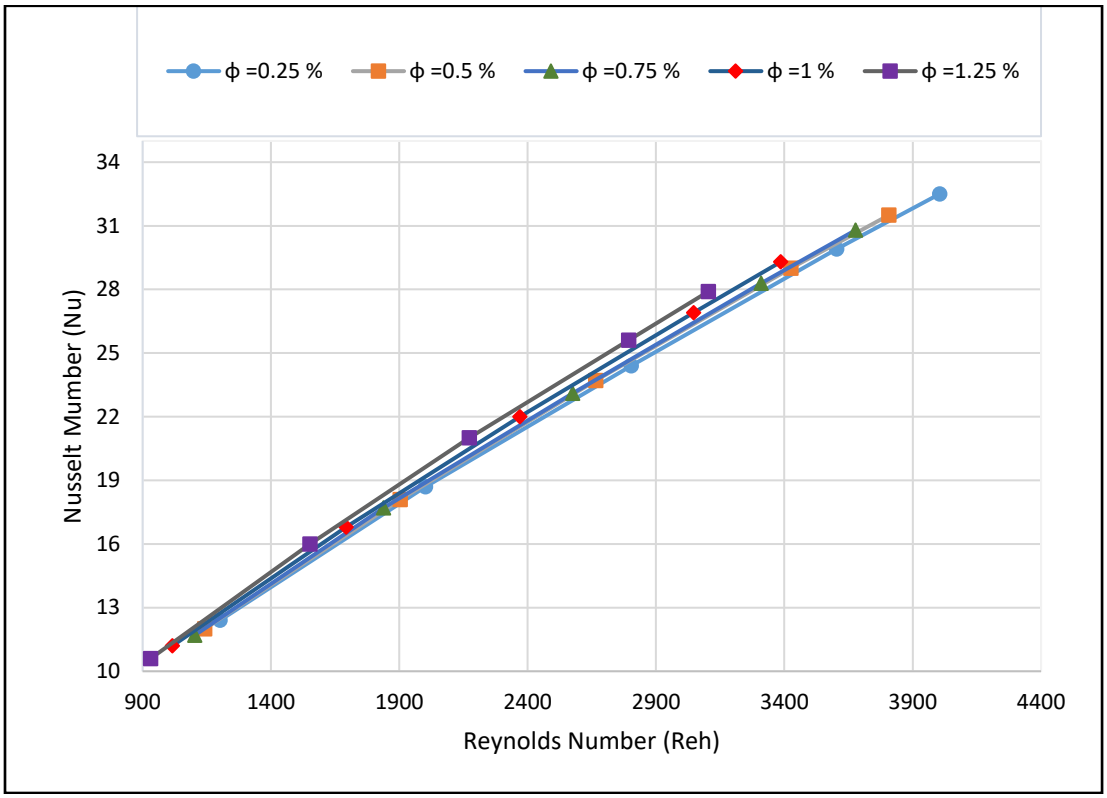


Figure 10 : Experimental Comparison of Nusselt and Reynolds Numbers for Finned Double-Pipe Heat Exchanger with Nanofluids

3.3. Overall Heat Transfer Coefficient (U)

The overall heat transfer coefficient (U) is an indication of the total thermal resistance encountered during the heat exchange process. In Figures 11 and 12 below, it can be observed that U increases monotonically with an increase in the fluid flow velocity (V_h = 3 – 10 L/min) and Al_2O_3 volume percentage (φ = 0.25 – 1.25 vol. %).

The smooth tube starts at U = 490.2 W/m²K at V_h = 3 L/min (Re_h = 1116) and reaches 634.7 W/m²K at 10 L/min (Re_h = 3720) for the base fluid (water) alone. Introducing nanofluid at φ = 1.25% increases U to 723.5 W/m²K, corresponding to a 48% enhancement over the baseline, primarily attributed to the increased effective thermal conductivity and nanoparticle-induced boundary layer disruption. The helically finned tube exhibits significantly higher performance. Under comparable conditions (φ = 1.25%, V_h = 10 L/min, Re_h = 3104), U reaches 1078.9 W/m²K.The combined effect of extended surface area and helical swirl enhances convective heat transfer more effectively than either mechanism alone.

Aghayari et al.,[28] reported 5–9.2% U enhancement at φ = 0.3 vol.% and $Re_h \approx$ 27,000. The present results indicate an enhancement of approximately 48%, achieved at nearly an order of magnitude lower Reynolds number (or pumping demand). This improvement is mainly attributed to operating at a stable nanoparticle concentration of 1.25 vol. % in combination with helical fin augmentation, at nearly an order of magnitude lower Reynolds number (or pumping demand) to enhance performance.

In contrast, the behavior of thermal effectiveness does not follow a linear trend with increasing nanoparticle concentration. This behavior can be explained by the combined influence of the combined influence of heat capacity rate ratios and fluid residence time, in addition to variations in the heat transfer coefficient. The finned configuration achieved a maximum effectiveness of 0.253, whereas the smooth tube exhibited values in the range of 0.167–0.214.

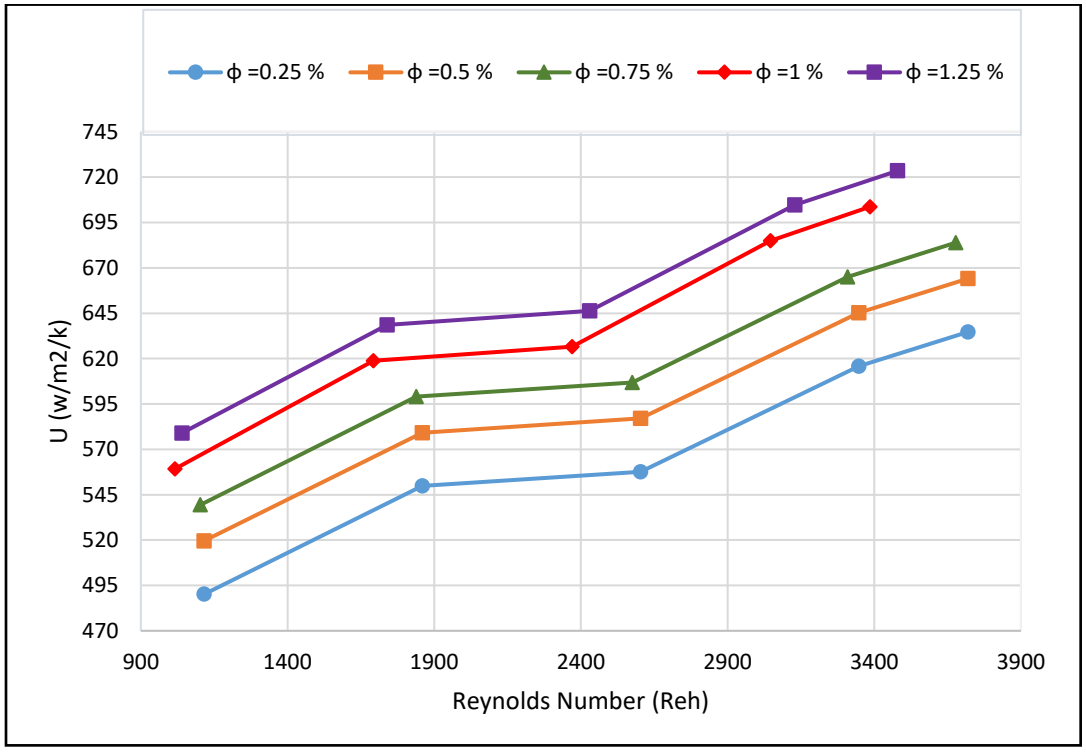


Figure 11: Overall heat transfer coefficient U versus hot-side Reynolds number Re_h for Smooth tube configuration

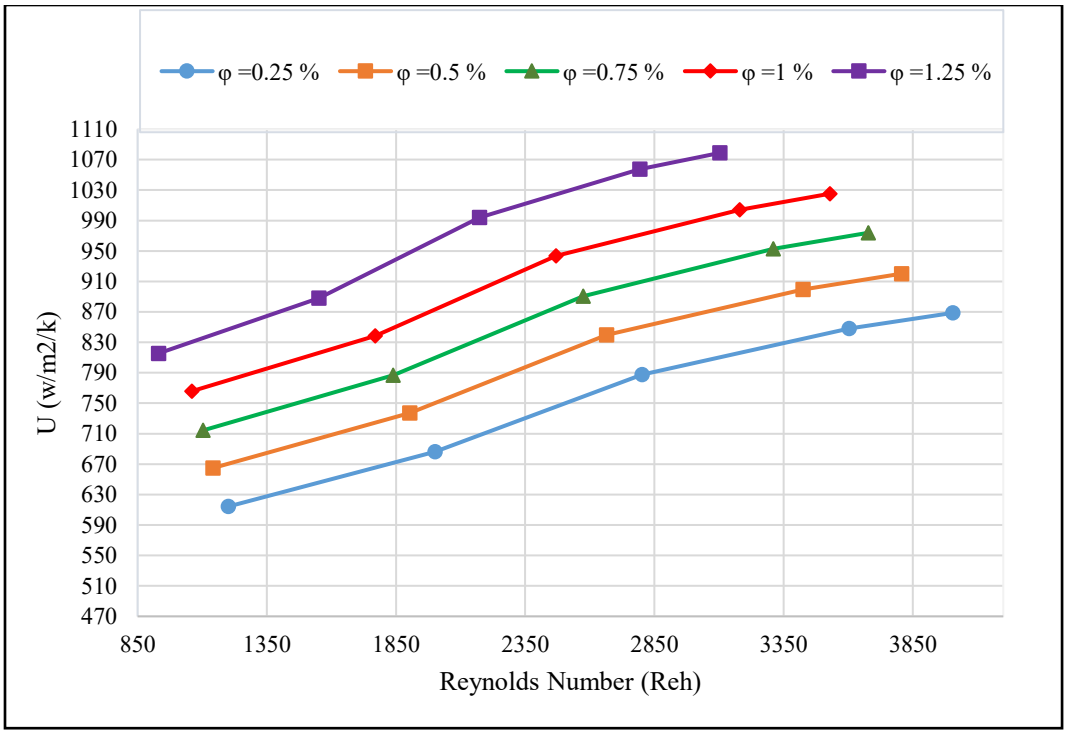


Figure 12 : Overall heat transfer coefficient U versus hot-side Reynolds number Re_h for Helically finned tube configuration.

3.4. Friction Factor Characteristics

The coefficient of friction decreases with increasing Reynolds number at all concentrations, as shown in Figures 13 and 14. The results for the smooth tube are in close agreement with the Blazius correlation, confirming the validity of the hydraulic measurements before extending the analysis to finned configurations.

In contrast, the tube with helical fins maintains higher coefficients of friction. The presence of helical fins in the annular gap increases the shape form resistance and enhances shear stress near the wall, while also inducing a secondary vortex that disrupts the axial momentum boundary layer. These combined effects result in a significant increase in the overall flow resistance. This increase becomes more pronounced with increasing nanoparticle concentration. At φ = 1.25% by volume, the interactions of aluminum oxide nanoparticles near the fin surfaces contribute to increased viscous dissipation, as indicated by pressure drop measurements. This effect is less pronounced at lower concentrations but remains more evident compared to the case of nanofluids in smooth tubes. Even with this increase, the scaling relationship is preserved, as expressed by $f \propto Re_h - n$.

This relationship is conserved under all tested conditions ($n \approx 0.25$). This indicates that the flow remains fully developed and that the additional resistance follows a predictable pattern. In practice, this behavior is advantageous. Although the hydraulic resistance increases, it does not become excessive, and the Performance Evaluation Criterion (PEC) values, which exceed one in most cases, demonstrate that the thermal improvement

outweighs the resistance increase. Under practical operating conditions, the combined use of helical fins and nanofluid represents a reasonable trade-off.

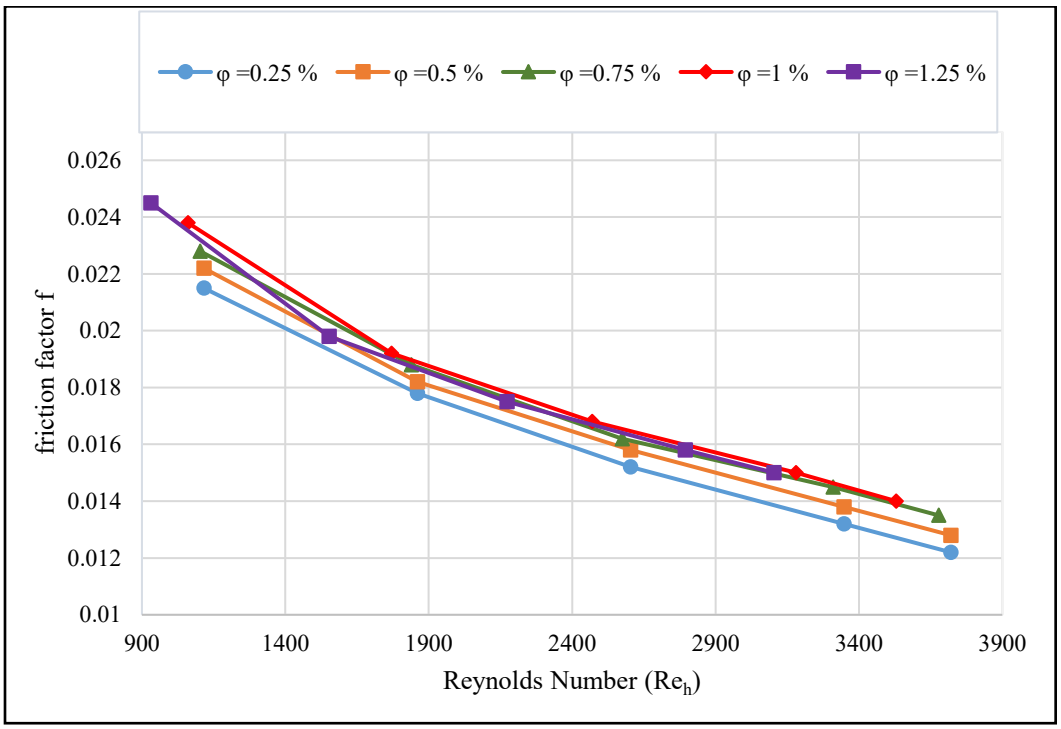


Figure 13: Friction factor versus hot-side Reynolds number for smooth double-pipe heat

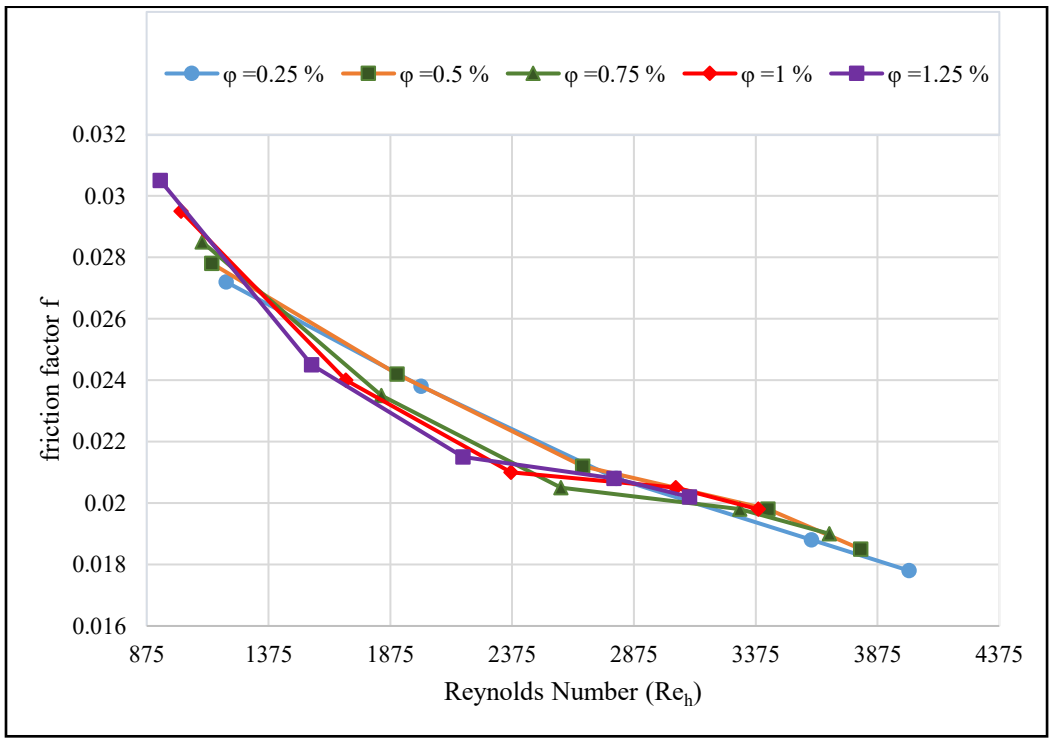


Figure 14: Friction factor versus hot-side Reynolds number finned double-pipe heat exchangers

3.5. Performance Evaluation Criterion (PEC) Analysis

The PEC criterion was employed to assess whether the thermal gains are justified by the pressure drop, reflecting a balance between the two factors. Figures 15, and 16 show that the PEC increases with increasing Reynolds number and Al_2O_3 concentration in both the smooth and finned configurations. The smooth tube values range from 0.72 to 1.82, while the finned tube yields considerably higher values, reaching 2.44 at $\varphi = 0.25\%$ and high Reynolds numbers, with most of the improved values remaining above 1. This indicates that the helical fins create secondary flows that replenish the fluid boundary layer near the heated wall, and it is precisely this replenishment that improves the balance between thermal and hydraulic performance. Increasing the nanoparticle concentration within the studied range further increases the PEC value, at least in the operating window where the convection gains exceed the increase in friction.

The Nusselt number (Nu_h) behavior does not follow a regular, monotonic trend. A non-monotonic response is observed; a concentration of $\varphi = 0.25\%$ significantly improves the Nusselt number on the hot side, but at $\varphi = 1.25\%$, a slight decrease is observed. This indicates what high particle density actually does to the fluid. The Al_2O_3 nanoparticles increase the dynamic viscosity of the fluid. This behavior was consistent with observations made during the preparation of samples at higher concentrations, which exhibited significantly greater flow resistance compared to the 0.25% concentration batches. The increased viscosity thickens the velocity boundary layer and dampens turbulence intensity. Beyond a certain loading threshold, these viscous effects become dominant, and the thermal conductivity gain can no longer compensate for them. The result is a marginal decrease in the overall heat transfer coefficient not severe, but consistent across all experimental iterations.

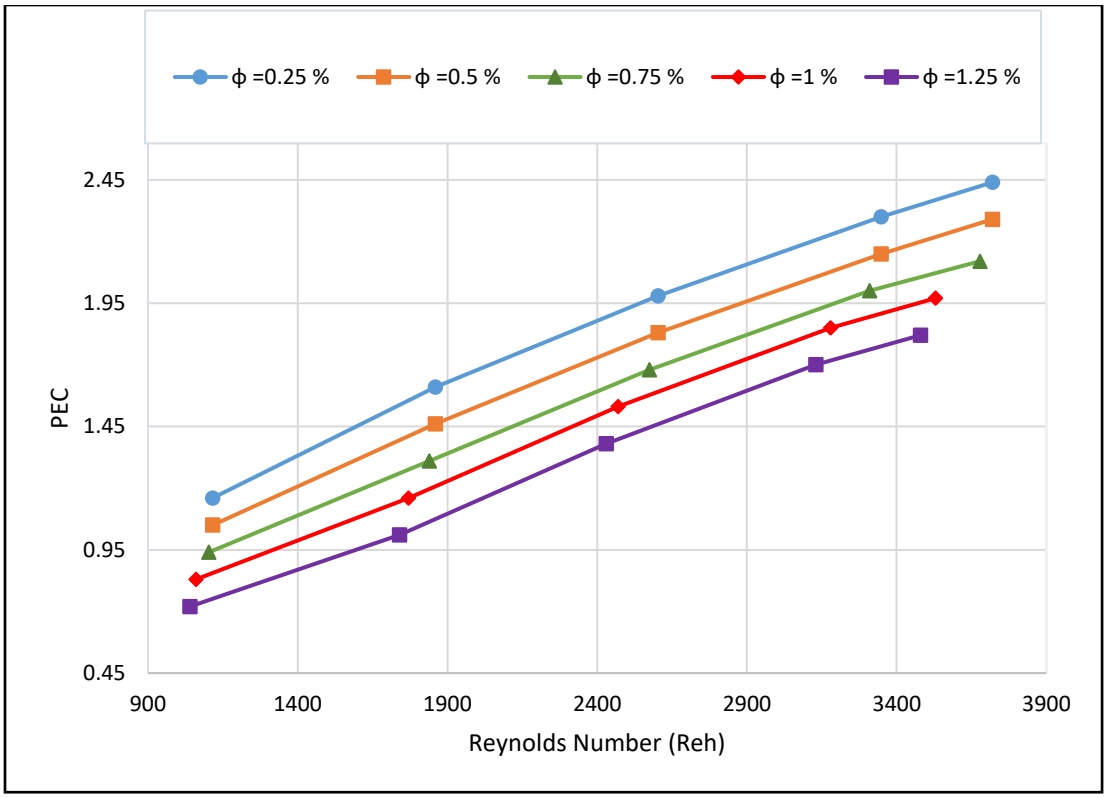


Figure 15: PEC versus hot-side Reynolds number for smooth double-pipe heat exchangers

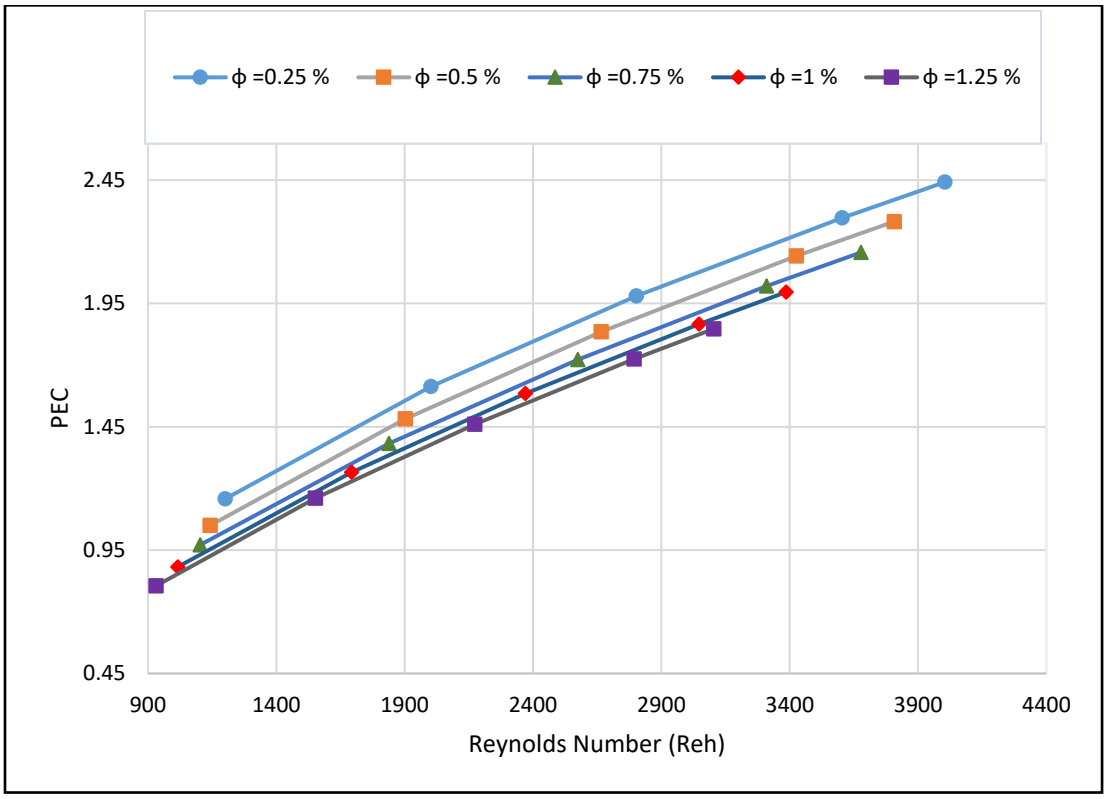


Figure 16: PEC versus hot-side Reynolds number finned double-pipe heat exchangers

4. Conclusions

This study evaluated the thermohydraulic performance of a double-pipe heat exchanger with helical fins, using an Al_2O_3/water nanofluid with volume fractions ranging from $\varphi = 0.25$ to 1.25%. The recorded improvements were consistent and quantifiable.

The Nusselt number in the finned configurations exceeded that of the smooth tube by 48–75%, reaching its maximum at $Re_h = 3104$ and $\varphi = 1.25\%$. The addition of the nanofluid contributed an additional 10–25% improvement across a flow range of $V_h = 3$–10 L/min. The overall heat transfer coefficient peaked at $U = 1079$ W/m²K under the same conditions, representing a 48% gain compared to the smooth tube value of $U = 724$ W/m²K.

The hydraulic penalty is real but manageable. The pressure drop increased by 25–35% in the finned cases, with a maximum value of 3.44 kPa remaining below 4 kPa in all cases, following the expected relationship of $f \propto Re_h^{-n}$. The PEC in approximately 85% of the finned test cases, with the highest recorded value being 2.44 at $\varphi = 0.25\%$ and $Re_h = 3720$, compared to a maximum value of 1.82 for the smooth tube. Under the tested conditions, the thermal gain consistently outweighed the pressure drop penalty.

The optimal operating point is located at $\varphi = 1.0$–1.25% by volume and $V_h = 9$–10 L/min ($Re_h \approx 3000$–3500), where the overall heat transfer coefficient (U) improvement reaches approximately 50%, and the PEC stabilizes around 2.0.

The present dataset contributes beyond the directly reported results. It represents one of the first experimental studies combining helical fins and nanofluids in a double-tube heat exchanger (DPHE) at low to medium Reynolds numbers, achieving nearly double the PEC compared to nanofluid configurations. Friction coefficients were derived directly from experimental measurements rather than theoretical assumptions, enhancing their applicability for CFD validation and scale-up applications. The required pumping power is reduced by approximately 60% compared to high Reynolds number configurations such as those reported by Aghayari et al. ($Re \approx 27{,}000$), a significant practical difference when considering the potential for retrofitting existing industrial systems.

5. Future Research Directions

Three directions stand out for future work. Hybrid nanofluids(Al_2O_3-SiC or CNT-Al_2O_3)offer something single-component systems simply cannot: the ability to tune rheological behavior and thermal conductivity independently. That independence is what makes pushing PEC beyond 3.0 a realistic target rather than a theoretical one. With single-component fluids, improving one property tends to compromise the other, and that tension is hard to escape.

Numerical modeling deserves serious attention here. The multiphase k-ω SST model, once benchmarked against the friction factor and Nusselt number data from this study, could systematically explore fin spacing and height combinations without the cost and time of

building a new rig for each case. Had this approach been available earlier, it would have meaningfully shortened the experimental timeline and might have pinned down the optimal fin pitch with a precision that experimental methods alone struggle to deliver.

Fouling, however, is the gap no one has closed yet. How does PEC hold up after extended operation? The present data offer no answer, and that answer matters before anyone takes this technology seriously at the industrial scale. Long-term experimental validation is not optional here, and any such campaign needs to build maintenance scheduling into the design from the start, not treat it as an afterthought.

From a purely practical standpoint, the concept has a lot going for it. No moving parts, no external power draw, no structural changes to existing pipework — these are not minor advantages when you are talking about retrofitting a live industrial system. Under the tested conditions, the configuration is a credible upgrade path for HVAC installations, process heating lines, and renewable energy setups where taking the system offline for redesign carries real cost. Much of the groundwork needed to move toward pilot-scale testing already exists in this study.

6. Reference

[1] V. N. Duy, T. N. Tien, D. V. Minh, and Q. K. Vu, "An experimental and Comparative performance of a thermal electric generator system using different heat exchanger fluids," *International Journal of Heat and Fluid Flow*, vol. 112, p. 109732, Mar. 2025, doi: 10.1016/j.ijheatfluidflow.2024.109732.

[2] S. Agrebi, B. Tashtoush, and A. Guizani, "Performance analysis of helical coil heat exchangers for latent heat thermal storage in solar applications," *Energy Conversion and Management*, vol. 343, p. 120205, Nov. 2025, doi: 10.1016/j.enconman.2025.120205.

[3] Naseema, S. NawazishMehdia, M. Manzoor Hussain, S. Khader Basha, and Mohd. Abdul Samad, "Heat Enhancement Of Heat Exchanger Using Aluminium Oxide(Al2o3), Copper Oxide(Cuo)Nano Fluids With Different Concentrations," *Materials Today: Proceedings*, vol. 5, no. 2, pp. 6481–6488, 2018, doi: 10.1016/j.matpr.2017.12.261.

[4] A. G *et al.*, "Study of impact of nano fluids on performance of microchannel heat exchangers using CFD," *International Journal of Thermofluids*, vol. 24, p. 100836, Nov. 2024, doi: 10.1016/j.ijft.2024.100836.

[5] S. S. Mousavi Ajarostaghi, M. Zaboli, H. Javadi, B. Badenes, and J. F. Urchueguia, "A Review of Recent Passive Heat Transfer Enhancement Methods," *Energies*, vol. 15, no. 3, p. 986, Jan. 2022, doi: 10.3390/en15030986.

[6] A. Alizadeh *et al.*, "Numerical and statistical analysis of hybrid nanofluid impact on finned shell and coil heat exchanger performance," *Journal of Engineering Research*, p. S2307187726000337, Feb. 2026, doi: 10.1016/j.jer.2026.02.005.

[7] S. Ahmad and H. A. Alsalmah, "Numerical and artificial intelligent analysis of double pipe heat exchanger exposed to solar irradiation for sustainable energy solutions," *Results in Engineering*, vol. 27, p. 105994, Sep. 2025, doi: 10.1016/j.rineng.2025.105994.

[8] S. H. Hashemi Karouei, D. J. Jasim, A. Basem, A. J. Sultan, A. H. Al-Rubaye, and S. S. Mousavi Ajarostaghi, "On the thermal performance of a shell and double coil heat exchanger: Numerical analysis of the geometrical characteristics impacts," *Case Studies in Thermal Engineering*, vol. 63, p. 105349, Nov. 2024, doi: 10.1016/j.csite.2024.105349.

[9] J. Huang *et al.*, "Multi-objective optimization of a double helical coil heat exchanger using response surface method and genetic algorithm," *International Journal of Thermal Sciences*, vol. 199, p. 108927, May 2024, doi: 10.1016/j.ijthermalsci.2024.108927.

[10] Y. E. Bizuneh, T. D. Asres, E. B. Gebresilassie, and A. E. Bizuneh, “Numerical Investigation on Heat Transfer of CuO-Water Nano-fluid in a circular pipe with twisted tape inserts,” Oct. 14, 2024, *In Review*. doi: 10.21203/rs.3.rs-5169697/v1.
[11] H. A. Al-Asadi *et al.*, “Innovative spiral fin design for convection improvement in double-coil heat exchangers: A simulation-based approach,” *International Communications in Heat and Mass Transfer*, vol. 174, p. 110936, May 2026, doi: 10.1016/j.icheatmasstransfer.2026.110936.
[12] M. Öztürk and E. Çiftçi, “Numerical analysis of a helically coiled tube heat exchanger performance utilized in molten salt nuclear reactors for molten salt and He-CO2 working fluid conditions,” *Progress in Nuclear Energy*, vol. 187, p. 105844, Sep. 2025, doi: 10.1016/j.pnucene.2025.105844.
[13] M. Hameed, M. S. Abbasi, A. H. Kazim, and A. Shabbir, “Thermal analysis of an Archimedean spiral-shaped circular piped heat exchanger with nano-fluids using simulation,” *Results in Engineering*, vol. 30, p. 110098, Jun. 2026, doi: 10.1016/j.rineng.2026.110098.
[14] H. T. Nam, S. Lee, M. Kong, and S. Lee, “Numerical Study of Flow and Heat Transfer Characteristics for Al2O3 Nanofluid in a Double-Pipe Helical Coil Heat Exchanger,” *Micromachines*, vol. 14, no. 12, p. 2219, Dec. 2023, doi: 10.3390/mi14122219.
[15] B. K. Ahirwar and A. Kumar, “Enhanced heat transfer using CuO+ZnO-water hybrid nanofluid with helical coil inserts in double pipe heat exchanger: Performance analysis and correlation development,” *International Journal of Thermal Sciences*, vol. 224, p. 110650, Jun. 2026, doi: 10.1016/j.ijthermalsci.2025.110650.
[16] L. Ben Said *et al.*, “Development of improved heat transfer of double helical pipe heat exchangers using nano-fluids and perforated curved tabulators,” *Case Studies in Thermal Engineering*, vol. 70, p. 106106, Jun. 2025, doi: 10.1016/j.csite.2025.106106.
[17] F. A. Ali, A. M. Alsaffawi, and K. H. Mohammed, “THE IMPACT OF ALUMINA NANOPARTICLES SUSPENDED IN ETHYLENE GLYCOL ON THE PERFORMANCE EFFICIENCY OF A DOUBLE PIPE HEAT EXCHANGER,” *Frontiers in Heat and Mass Transfer*, vol. 15, Dec. 2020, doi: 10.5098/hmt.15.21.
[18] R. A. Rinik, A. A. Bhuiyan, and Md. R. Karim, “Enhancement of heat transfer using elliptical twisted inner pipe with convergent conical ring turbulator for turbulent flow in double pipe heat exchanger,” *International Journal of Thermal Sciences*, vol. 210, p. 109558, Apr. 2025, doi: 10.1016/j.ijthermalsci.2024.109558.
[19] Y. Cao, H. Ayed, H. S. Dizaji, M. Hashemian, and M. Wae-hayee, “Entropic analysis of a double helical tube heat exchanger including circular depressions on both inner and outer tube,” *Case Studies in Thermal Engineering*, vol. 26, p. 101053, Aug. 2021, doi: 10.1016/j.csite.2021.101053.
[20] M. E. Nakhchi, M. Hatami, and M. Rahmati, “Experimental investigation of performance improvement of double-pipe heat exchangers with novel perforated elliptic turbulators,” *International Journal of Thermal Sciences*, vol. 168, p. 107057, Oct. 2021, doi: 10.1016/j.ijthermalsci.2021.107057.
[21] Z. Piran, S. S. Mousavi Ajarostaghi, and M. Farhadi, “Impact of employing twisted tube with spiral V-shaped axial fins on the charging performance inside a phase change material storage: Numerical examination,” *Journal of Energy Storage*, vol. 100, p. 113645, Oct. 2024, doi: 10.1016/j.est.2024.113645.
[22] S. A. Zonouzi, “Accelerated solidification process in a compact helical thermal energy storage system using two-pass flow and axial fins,” *Thermal Science and Engineering Progress*, vol. 73, p. 104632, May 2026, doi: 10.1016/j.tsep.2026.104632.
[23] A. A. Badr, M. T. Luhaibi, T. A. D. M. S. Almula, and A. S. Abedalh, “Thermophysical performance enhancement of vapor-compression chiller systems via metal oxide nanofluid integration,” *Env Prog and Sustain Energy*, vol. 45, no. 1, p. e70255, Jan. 2026, doi: 10.1002/ep.70255.
[24] Y. Peng, Y. Tao, Z. Zhou, Y. Wang, and J. Tu, “Experimental investigation on thermo-hydraulic performance of Al2O3–water, CuO–water and MWCNT–water in a double-tube helically coiled heat exchanger,” *International Journal of Thermal Sciences*, vol. 210, p. 109628, Apr. 2025, doi: 10.1016/j.ijthermalsci.2024.109628.
[25] S. Yousefi, M. Mahdavi, S. Soheil Mousavi Ajarostaghi, and M. Sharifpur, “Hydrothermal behavior of nanofluid flow in a microscale backward-facing step equipped with dimples and ribs; Lattice Boltzmann method approach,” *Thermal Science and Engineering Progress*, vol. 43, p. 101987, Aug. 2023, doi: 10.1016/j.tsep.2023.101987.

[26] F. M. Hussien, J. J. Faraj, and A. J. Hamad, “Experimental Investigation of Double Pipe Heat Exchanger Performance based on Alumina and Copper Oxide Working Nanofluids,” *IOP Conf. Ser.: Mater. Sci. Eng.*, vol. 1105, no. 1, p. 012061, Jun. 2021, doi: 10.1088/1757-899X/1105/1/012061.
[27] Y. H. Assaf, A. Akroot, K. Alnamasi, and M. A. Ismail, “Investigation of heat transfer performance in heat exchangers using hybrid nanofluids and twisted tape inserts with fixed special rings,” *Sci Rep*, vol. 15, no. 1, p. 18450, May 2025, doi: 10.1038/s41598-025-02135-3.
[28] R. Aghayari, H. Maddah, M. Zarei, M. Dehghani, and S. G. Kaskari Mahalle, “Heat Transfer of Nanofluid in a Double Pipe Heat Exchanger,” *International Scholarly Research Notices*, vol. 2014, pp. 1–7, Nov. 2014, doi: 10.1155/2014/736424.
[29] P. K. Chaurasiya, J. Heeraman, S. K. Singh, T. N. Verma, G. Dwivedi, and A. K. Shukla, “Exploring the combined influence of primary and secondary vortex flows on heat transfer enhancement and friction factor in a dimpled configuration twisted tape with double pipe heat exchanger using SiO2 nano fluid,” *International Journal of Thermofluids*, vol. 22, p. 100684, May 2024, doi: 10.1016/j.ijft.2024.100684.
[30] S. K. Gaur and R. R. Sahoo, “Heat Transfer Augmentation in Multi-Tube Heat Exchangers for Decarbonization: Optimizing Straight/Helical Fin,” *Journal of Thermal Science and Engineering Applications*, vol. 18, no. 9, p. 091011, Sep. 2026, doi: 10.1115/1.4071196.
[31] S. M. Mousavi, A. Sheikhi Azizi, M. Razbin, A. A. Rabienataj Darzi, and M. Li, “Optimized design of Helical-Finned Double Pipe heat exchangers via numerical simulation and Artificial Intelligence,” *Applied Thermal Engineering*, vol. 258, p. 124605, Jan. 2025, doi: 10.1016/j.applthermaleng.2024.124605.
[32] U. E. Inyang and I. J. Uwa, “Heat Transfer in Helical Coil Heat Exchanger,” *ACES*, vol. 12, no. 01, pp. 26–39, 2022, doi: 10.4236/aces.2022.121003.
[33] F. B. Daşbaş, A. Çutay, and M. Paksoy, “A Review of CFD Applications in Spiral and Helical Heat Exchangers”.
[34] B. Erdoğan and Ç. Ç. Bayar, “Bridging Molecular Modeling Insights and Experimental Findings: A Comparative Study on Surfactant Effects in Al2O3 Nanofluids,” *Nanomaterials*, vol. 16, no. 2, p. 92, Jan. 2026, doi: 10.3390/nano16020092.
[35] A. Altun, O. Şara, and S. Doruk, “SDS SURFACTANT EFFECTS ON STABILITY AND THERMOPHYSICAL PROPERTIES OF Al2O3–WATER BASED NANOFLUIDS,” *Konya Journal of Engineering Sciences*, vol. 10, no. 3, pp. 599–612, Sep. 2022, doi: 10.36306/konjes.1019424.
[36] D. Majidi, H. Alighardashi, and F. Farhadi, “Experimental studies of heat transfer of air in a double-pipe helical heat exchanger,” *Applied Thermal Engineering*, vol. 133, pp. 276–282, Mar. 2018, doi: 10.1016/j.applthermaleng.2018.01.057.
[37] S. Eiamsa-ard and P. Promvonge, “Thermal characteristics in round tube fitted with serrated twisted tape,” *Applied Thermal Engineering*, vol. 30, no. 13, pp. 1673–1682, Sep. 2010, doi: 10.1016/j.applthermaleng.2010.03.026.
[38] W.-T. Ji, D.-C. Zhang, Y.-L. He, and W.-Q. Tao, “Prediction of fully developed turbulent heat transfer of internal helically ribbed tubes ? An extension of Gnielinski equation,” *International Journal of Heat and Mass Transfer*, vol. 55, no. 4, pp. 1375–1384, Jan. 2012, doi: 10.1016/j.ijheatmasstransfer.2011.08.028.
[39] N. Ben Khedher, S. A. M. Mehryan, M. Medani, M. M. Selim, N. B. M. Elbashir, and M. Boujelbene, “Enhancing the efficiency of a double tube heat exchanger via a novel vibrating woven wire turbulator combined with a helical coiled wire; an experimental study,” *Applied Thermal Engineering*, vol. 248, p. 123121, Jul. 2024, doi: 10.1016/j.applthermaleng.2024.123121.
[40] M. K. Bhatnagar, M. Rai, M. Ashraf, O. Kapoor, T. G. Mamatha, and M. Vishnoi, “Efficiency enhancement of heat exchanger using inserts and nano-fluid - A review,” *Materials Today: Proceedings*, vol. 44, pp. 4399–4403, 2021, doi: 10.1016/j.matpr.2020.10.575.
[41] N. S. Reddy, K. Rajagopal, and P. H. Veena, “Experimental Investigation of Heat Transfer Enhancement of a Double Pipe Heat Exchanger with Helical Fins in the Annulus Side”.

Nomenclature

Symbol	Definition	Unit
A	Area of heat transfer surface	m^2
C_p	Specific heat capacity	J/kg.K
D_h	Hydraulic diameter	m
L	Test section length	m
LMTD	Logarithmic mean temperature difference	K
N	Number of fins	-
Nu	Nusselt number	-
Nu_0	Baseline Nusselt number	-
P	Pressure drop	Pa
PEC	Performance Evaluation Criterion	-
Q	Heat transfer rate	W
Q_{act}	Actual heat transfer	W
Q_{avg}	Average heat transfer rate	W
Q_c	Cold-side heat transfer rate	W
Q_h	Hot-side heat transfer rate	W
Q_{max}	Maximum possible heat transfer	W
Re	Reynolds number	-
U	Overall heat transfer coefficient	W/m^2. K
V	Mean velocity	m/s
d_i	Inner tube diameter	m
d_o	Outer diameter	m
f	Friction factor	-
h	Fin height	mm
h_i	Inner-side heat transfer coefficient	W/m^2. K
h_o	Outer-side heat transfer coefficient	W/m^2. K
k	Thermal conductivity	W/m. K
k_{wall}	Wall thermal conductivity	W/m. K
$\dot{m}$	Mass flow rate	Kg/s
mu	Dynamic viscosity	Pa.s
p	Fin pitch / spacing	mm
ρ	Density	Kg/m^3
t	Fin thickness / wall thickness	mm